Editors' Suggestion

Heat Equilibration of Integer and Fractional Quantum Hall Edge Modes in Graphene

G. Le Breton,[1] R. Delagrange,[1] Y. Hong,[2] M. Garg,[1] K. Watanabe,[3] T. Taniguchi,[3] R. Ribeiro-Palau,[2] P. Roulleau,[1] P. Roche,[1] and F. D. Parmentier[1]

[1]*Université Paris-Saclay, CEA, CNRS, SPEC, 91191 Gif-sur-Yvette cedex, France*

[2]*Université Paris-Saclay, CNRS, Centre de Nanosciences et de Nanotechnologies (C2N), 91120 Palaiseau, France*

[3]*National Institute for Materials Science, 1-1 Namiki, 305-0044 Tsukuba, Japan*

(Received 27 April 2022; accepted 1 August 2022; published 8 September 2022)

Hole-conjugate states of the fractional quantum Hall effect host counterpropagating edge channels which are thought to exchange charge and energy. These exchanges have been the subject of extensive theoretical and experimental works; in particular, it is yet unclear if the presence of integer quantum Hall edge channels stemming from fully filled Landau levels affects heat equilibration along the edge. In this Letter, we present heat transport measurements in quantum Hall states of graphene demonstrating that the integer channels can strongly equilibrate with the fractional ones, leading to markedly different regimes of quantized heat transport that depend on edge electrostatics. Our results allow for a better comprehension of the complex edge physics in the fractional quantum Hall regime.

DOI: 10.1103/PhysRevLett.129.116803

The fractional quantum Hall (QH) effect emerges when a two-dimensional electron system is subjected to a strong perpendicular magnetic field B such that the filling factor $\nu = n_e h/eB$ takes fractional values (n_e is the carrier density, h Planck's constant, and $-e$ the electron charge). For hole-conjugate states, it takes the form $\nu = N_0 + 1 - p/q$, with N_0 the integer part of ν corresponding to fully filled Landau levels (LLs), q an odd number, and p such that $p/q < 1/2$. The edge structure for such states has been the subject of more than 30 years of research, originally focused on $\nu = 2/3$ (such that $N_0 = 0$ and $p/q = 1/3$) [1,2]. Some of the earlier works proposed the $\nu = 2/3$ edge to be composed of one downstream channel with integer electrical conductance $G_0 = e^2/h$ along with one *upstream* channel with fractional conductance $-1/3 \times G_0$ [2]. It was later proposed that interchannel interactions and disorder-assisted charge tunneling between the downstream and upstream channels radically change that structure. Strong interactions give rise to a downstream charged mode with fractional electrical conductance $2/3 \times G_0$ and one upstream *neutral* mode which only carries heat in the direction opposite to that of charge transport [3]. This *charge equilibration* was then generalized to other fractions [4,5]. Importantly, depending on ν the numbers of downstream fractional-charged modes and upstream neutral modes are not necessarily equal. Following their first observation [6], neutral modes were extensively investigated using shot noise [7–9] and local thermometry [10] measurements.

Recently, the question of *heat equilibration* between neutral and charged modes has been the center of a growing number of works, both experimental [11–14] and theoretical [15–20]. While most experiments confirm a charge equilibration (see, e.g., Refs. [21,22] for notable exceptions), heat equilibration is much less universal. In gallium arsenide (GaAs) based two-dimensional electron gases, partial to full heat equilibration was first reported at $\nu = 2/3, 3/5, 4/7$ [11], and $8/3$ [12]; however, a recent experiment showed an absence of heat equilibration at $\nu = 2/3$ even for large ($>300\ \mu$m) lengths [14]. Experiments in graphene reported no heat equilibration at $\nu = 5/3$ and $8/3$ [13] over a few microns scale, and, very recently, the observation of a temperature-induced heat equilibration at $\nu = 2/3$ and $3/5$ [23]. This diversity of observations is currently understood by the facts that the charge and heat equilibration lengths can be largely different depending on the coupling between the counterpropagating edge modes [13], and that the ratio between the number of coupled downstream modes N_d and upstream modes N_u strongly affects the equilibration. Namely, for states with $N_d = N_u$ (e.g., $\nu = 2/3$), heat equilibration is predicted to have slow algebraic length dependence [18,19,23], and is not observed at low temperature, even at large length scales [14]. On the contrary, for $N_d \neq N_u$ it should be exponentially fast [18,19,23]. However, it is still unclear whether, for fractional $\nu > 1$, the N_0 integer edge channels (ECs) stemming from the fully filled LLs participate in the heat equilibration along the edge [17]. If so, one should include them in the N_d downstream modes, which can lead to $N_d \neq N_u$ in states where $\nu = N_0 + 2/3$, radically changing heat equilibration.

We addressed this question by probing heat transport in graphene at filling factor $\nu = 8/3$. Figure 1(a) shows its edge structure, with $N_0 = 2$ integer ECs stemming from the fully filled zeroth LL, and a $\nu = 2/3$-like pair of counterpropagating fractional edge modes [17]. The upstream

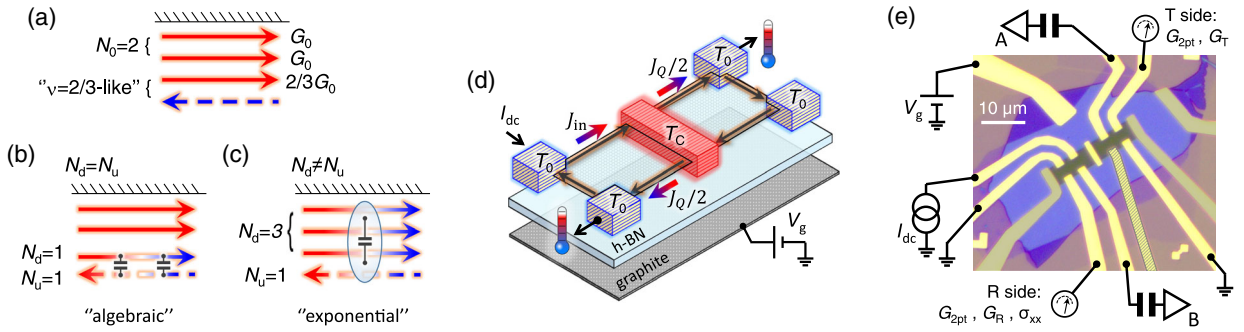

FIG. 1. $\nu = 8/3$ edge structure, without heat equilibration (a), with heat equilibration between fractional modes only (b), and between all modes (c). Full and dashed arrows: charged and neutral modes, with their chirality. Arrow color: temperature gradient in the presence of a temperature bias: hot source (red) on the left, cold source (blue) on the right. (d) Schematic representation of the experiment, with cold electrodes (blue) at T_0 and the metallic island (red) at T_c. Red arrows: chiral edge channels, gradient-colored arrows: heat flows going in ($J_{\rm in}$) and out of (J_{mQ}) the island. (e) Optical micrograph of the sample, with the experimental wiring. The encapsulated graphene flake is shown in green. The grayed out electrodes are left floating, and the hatched electrode is used as a current feed in cooldown 2.

mode can either exchange heat with only the fractional downstream mode [Fig. 1(b)]. This "algebraic" case is similar to $\nu = 2/3$, with $N_d = N_u = 1$, such that no heat equilibration is expected at low temperature and short or moderate lengths [13,14,23]. Conversely, the upstream mode can exchange heat with all downstream channels [Fig. 1(c)], such that $N_d = N_0 + 1 = 3$ and $N_u = 1$, implying a much more efficient heat equilibration. This difference is directly reflected in the heat flow, affecting the number N of effective ballistic heat transport channels [5,13,18,19]. In the nonequilibrated (algebraic) case, all downstream and upstream modes are ballistic and contribute independently, yielding $N = 4$. In the fully equilibrated case, the upstream mode suppresses heat transport down to $N = 2$.

Figure 1(d) shows our experimental principle. It was first demonstrated in GaAs in the integer QH regime [24], and later applied to the fractional QH effect [11,12]. Recent experiments [13,23,25] have extended it to graphene. A two-dimensional electron gas (here in graphene) is divided in two regions electrically connected by a floating metallic island, highlighted in red in Fig. 1(b). A perpendicular magnetic field B allows reaching the QH regime, with equal ν in both regions. The dc electrical current $I_{\rm dc}$ is applied to one of the cold electrodes [in blue in Fig. 1(d)], and flows downstream via the ECs [red lines in Fig. 1(d)] to the island. The latter evenly splits the current between the outgoing ECs in the two regions, resulting in a net Joule power directly dissipated into the island $J_{\rm in} = I_{\rm dc}^2/(4\nu G_0)$ [24–26]. This induces an increase in the electron temperature T_c of the island, while all other electrodes remain at base electron temperature T_0. The input heat flow $J_{\rm in}$ is evacuated from the island through the outgoing ECs on both sides of the island, each side carrying half of the outgoing heat flow, $J_{mQ}/2$. Each ballistic channel carries a quantum-limited heat flow $J_Q^e = 0.5\kappa_0(T_c^2 - T_0^2)$ [24,31,32], with $\kappa_0 = \pi^2 k_B^2/3h$ (k_B is Boltzmann's constant). Neglecting other contributions (e.g., coupling to phonons, see below), the heat balance simply reads $J_{mQ} = J_{\rm in}$, hence

$$J_{mQ} = \frac{1}{4\nu G_0} I_{\rm dc}^2 = 2N\frac{\kappa_0}{2}(T_c^2 - T_0^2), \qquad (1)$$

where N is the number of ballistic heat-carrying channels flowing out of each side of the island (the total number thus being $2N$). For integer QH states, N equals the filling factor ν. For hole-conjugate fractional QH states, N reflects the heat equilibration along the edge, as detailed above. N can be directly extracted by measuring the temperature T_c and comparing it to the input heat flow according to Eq. (1).

Figure 1(e) shows our implementation in a hexagonal boron nitride (h-BN)-encapsulated monolayer graphene sample. The charge carrier type and density are tuned using a graphite back gate upon which the voltage V_g is applied. The Ti/Au metallic island has dimensions 6.8 μm × 1.25 μm × 100 nm, its distance to the closest electrodes is ∼2.5 μm, and the width of the device is ∼5 μm. ECs flowing out of the two sides of the island, denoted "reflected" (R) and "transmitted" (T) with respect to the current feed, connect to measurement electrodes in this order: noise, low-frequency conductance, cold ground. We characterize charge transport by measuring the two-point differential conductances $G_{\rm 2pt} = (dV_{R,T}/d\tilde{I}_{R,T})^{-1}$ ($\tilde{I}_{R,T}$ are the currents directly applied to the measurement contacts on the R and T side), the differential transmitted and reflected transconductances $G_{R,T} = (dV_{R,T}/dI_{\rm dc})^{-1}$ probing current redistribution at the island, and the "longitudinal-like" differential conductance $\sigma_{xx} = G_0^2 \times dV_R/d\tilde{I}_T$. The latter vanishes for well-defined QH states because the chiral paths connecting the conductance measurement electrodes are interrupted by a cold ground. The island's electron temperature increase ΔT_c induces current fluctuations

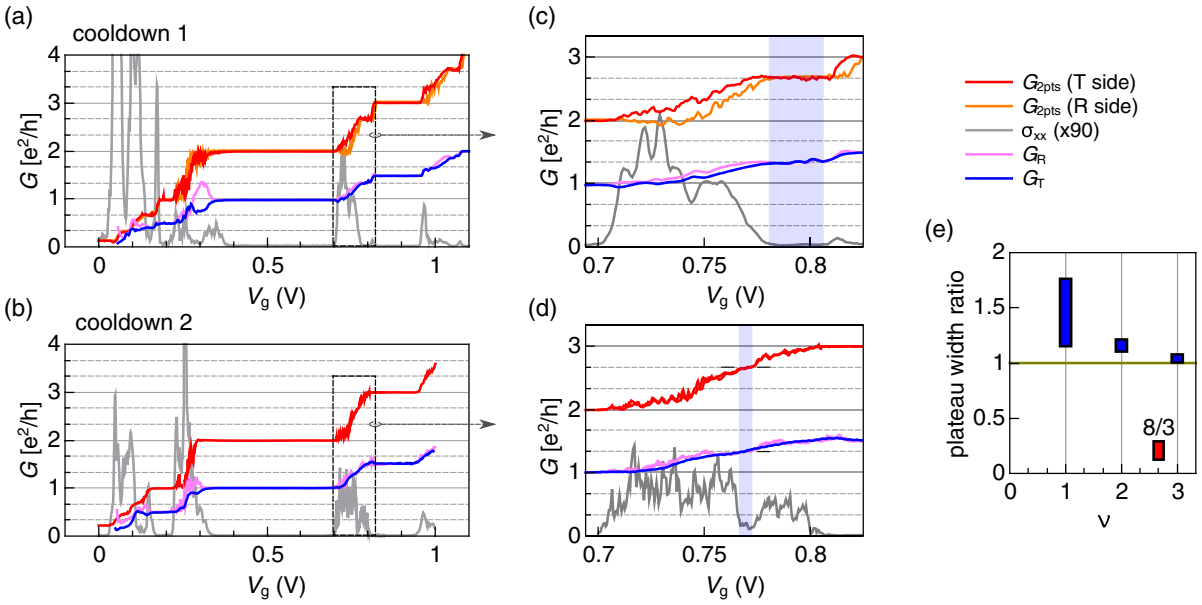

FIG. 2. Conductances versus V_g, measured at $B = 7$ T and $T = 10$ mK for (a) cooldown 1 and (b) cooldown 2. Red (respectively, orange): two-point conductance $G_{2\mathrm{pt}}$ of the transmitted (respectively, reflected) side (see legend on the upper right corner). Gray: longitudinal-like conductivity σ_{xx}. Lavender: reflected transconductance G_R. Blue: transmitted transconductance G_T. (c),(d) Close-ups of the $\nu = 2 \to 3$ transition [dashed rectangles in (a) and (b)]. The $\nu = 8/3$ region is highlighted in blue. Horizontal ticks in (d): guides for the eyes at the expected values of $G_{2\mathrm{pt}}$ and $G_{T/R}$. (e) Ratio between the V_g widths of the $\nu = 1, 2, 3$ (blue) and $\nu = 8/3$ (red) plateaus between cooldown 2 and cooldown 1. The maximum of the bars corresponds to the ratio of the widths extracted from $G_{2\mathrm{pt}}$, and the minimum to the one extracted from σ_{xx}.

$\Delta S = \nu G_0 k_B \Delta T_c$ in the ECs flowing out of the island, that we detect through two independent noise measurement lines on each side [A and B in Fig. 1(e)].

We present measurements in two consecutive cooldowns of the same device. All connections were kept identical, except for the current feed which was swapped between the R side in cooldown 1 (CD1) and the T side in cooldown 2 (CD2).

Figure 2 shows conductance measurements as a function of the gate voltage, obtained at $B = 7$ T, for CD1 [Figs. 2(a) and 2(c)] and CD2 [Figs. 2(b) and 2(d)]. Well-defined QH states, at both integer and fractional ν, are characterized by quantized plateaus in the two-point conductances $G_{2\mathrm{pt}} = \nu G_0$, along with a vanishing σ_{xx}. On most of these plateaus (except notably on $\nu = 1/3$ in CD2), G_R and G_T have equal values, quantized to $0.5 \times \nu G_0$, indicating chiral charge transport and near-ideal current redistribution at the island. Figures 2(c) and 2(d) show a close-up of the $\nu = 2 \to 3$ transition. The width of the $\nu = 8/3$ plateau is strongly reduced in CD2, with a nonzero local minimum in σ_{xx}. Nevertheless, chirality and current redistribution are still preserved: both transconductances are equal, with a plateau at half-quantized value $0.5 \times 8/3 G_0$ [26]. We superimpose two traces in Fig. 2(d), illustrating the reproducibility of this feature.

Figure 2(e) plots the ratio between the V_g widths of the plateaus between CD2 and CD1. These spans can be extracted from the quantized $G_{2\mathrm{pt}}$, or from the minima in σ_{xx}; either show that for CD2, all integer QH plateaus are wider while $\nu = 8/3$ is markedly narrower. The V_g position of each plateau can be similarly extracted [26]; we observe a systematic shift towards more negative V_g at CD2, corresponding to an increased intrinsic electron doping $\Delta n_e \approx 1.7 \times 10^{10}$ cm^{-2}.

Thermal measurements were performed for each QH state in which the chirality and current redistribution criteria are enforced: $\nu = \{1/3, 1, 2, 8/3, 3\}$ for CD1, and $\nu = \{1, 2, 8/3, 3\}$ for CD2. We use auto- and cross-correlations of the two noise lines to extract ΔT_c from spurious noise contributions [26,33]. Figure 3 shows ΔT_c measured as a function of the dc current I_{dc}. All filling factors display the same qualitative behavior, in agreement with Eq. (1), where ΔT_c increases linearly beyond a thermal rounding at low I_{dc}. Following Eq. (1), the slope only depends on $1/\sqrt{N \times \nu}$. The data show similar slopes for both cooldowns, except $\nu = 8/3$, with a markedly higher slope at CD2. This observation, discussed in detail below, is the main result of our work. Note that for this last dataset, we kept I_{dc} small, as both autocorrelations became different above $|I_{\mathrm{dc}}| \approx 1$ nA [26].

We compared our data to Eq. (1), assuming negligible electron-phonon cooling in the island. This is reasonable given its small volume and the very low temperatures [26]; previous experiments in graphene [13,23,25], with similar dimensions, also reported negligible electron-phonon cooling. Equation (1) appears as black lines in Fig. 3.

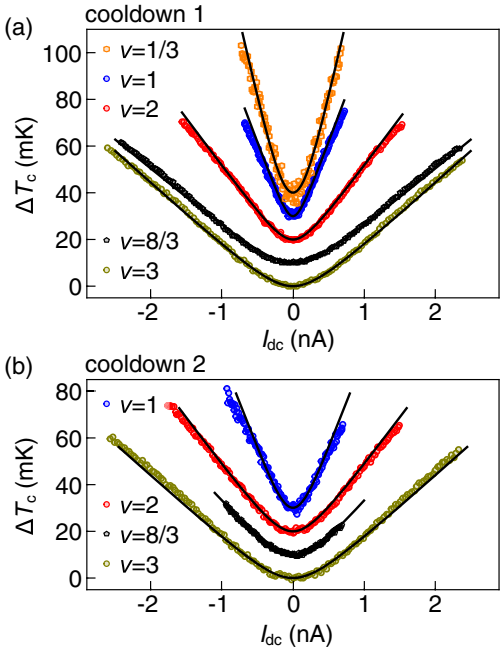

FIG. 3. ΔT_c versus I_{dc}, for cooldown 1 (a) and 2 (b). Symbols: experimental data (orange ⬡: $\nu = 1/3$; blue ○: $\nu = 1$; red ○: $\nu = 2$; black ⬠: $\nu = 8/3$; dark yellow ○: $\nu = 3$). Black lines: fits (see text). Data and fits corresponding to each ν are vertically shifted by increments of 10 mK for clarity.

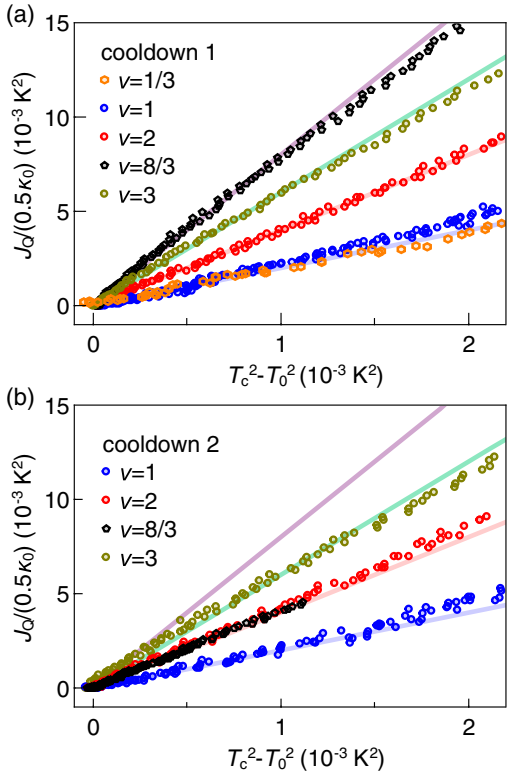

FIG. 4. Heat flow J_{mQ} in units of $\kappa_0/2$ versus $T_c^2 - T_0^2$, for cooldown 1 (a) and 2 (b). Symbols: experimental data corresponding to the one in Fig. 3 (orange ⬡: $\nu = 1/3$; blue ○: $\nu = 1$; red ○: $\nu = 2$; black ⬠: $\nu = 8/3$; dark yellow ○: $\nu = 3$). Lines: theoretical predictions for the quantized heat flow carried by $2N$ ballistic channels, with $N = 1$ (light blue), $N = 2$ (pink), $N = 3$ (light green), and $N = 4$ (lavender).

The number of ballistic heat carrying modes N is fixed to its expected value ($N = \nu$ for integer QH states, see below for $\nu = 8/3$), yielding an excellent agreement with the slope of the data. The thermal rounding is reproduced by adjusting the base electron temperature T_0 for each ν. These extracted T_0 match with the equilibrium Johnson-Nyquist noise measured at $I_{\mathrm{dc}} = 0$ [26]. For CD1, $T_0 \approx 12$ mK (for a fridge base temperature of 8.7 mK), with the notable exception of $\nu = 1/3$, where $T_0 \approx 42$ mK. For CD2, $T_0 \approx 15$ mK, except at $\nu = 1$, where $T_0 \approx 20$ mK. We attribute those variations, particularly the increase at lower ν, to mechanical vibrations [34]. Additional analysis (e.g., heat Coulomb blockade effects [35]), described in [26], yields a reasonable uncertainty on the extracted T_0 of about ± 3 mK, translating into a typical uncertainty on N of about ± 0.1.

The relation between the slopes in $\Delta T_c(I_{\mathrm{dc}})$ and quantized heat transport appears clearly when replotting the data in terms of the total heat flow leaving the island $J_{mQ} = I_{\mathrm{dc}}^2/(4\nu G_0)$ as a function of $(T_c^2 - T_0^2)$. This is shown in Fig. 4, with T_0 extracted from the above procedure, such that the data (J_{mQ} is plotted in units of $0.5\kappa_0$) naturally fall onto lines with integer slope $2N$. The representation of Fig. 4 shows heat transport properties of each filling factor regardless of charge transport. As a striking example, the data at $\nu = 1/3$ and $\nu = 1$ fall onto the same $N = 1$ line, demonstrating that a fractional and an integer ECs carry the same universally quantized heat flow $\pi^2 k_B^2/6h(T_c^2 - T_0^2)$ [31,32], previously reported in GaAs [11] and graphene [23,25]. Figure 4 emphasizes the remarkable difference between both cooldowns for $\nu = 8/3$. On the one hand, in CD1 we observe a quantized heat flow with $N = 4$ channels, corresponding to nonequilibrated ballistic heat transport through all downstream charged modes and the upstream neutral mode. This is consistent with recent results in bilayer graphene [13]. On the other hand, for CD2, $\nu = 8/3$ falls on top of $\nu = 2$, corresponding to a quantized heat flow with $N = 2$ channels. This unambiguously signals a strong heat equilibration at $\nu = 8/3$, corresponding to the upstream neutral mode fully equilibrating with both integer and fractional downstream charged modes.

The increase of disorder and doping revealed in Fig. 2 thus leads to a large change in the thermal conductance of $\nu = 8/3$ between the two cooldowns. This strongly suggests that heat equilibration in CD2 is exponential, confirming the fact that the integer ECs have to be considered in this equilibration process. Microscopically, the increase electron doping, likely stemming from charged impurities adsorbed at the surface of the sample while it was exposed to ambient air during thermal cycling, can favor efficient

equilibration. Indeed, these impurities locally increase the electron density in the vicinity of the edge, resulting in a sharper edge confinement potential which increases the coupling between the more closely packed ECs. Not only can the increased coupling drive the heat equilibration in an exponential regime, but it can also drastically affect the characteristic length [23], further favoring equilibration. Even though spatially separated [17], the fractional and integer channels can thus be strongly coupled; interestingly, this can be related to recent observations of charge tunneling between integer channels at $\nu = 3$ in graphene [36,37].

Finally, the small, nonzero σ_{xx} measured in CD2 raises the question whether our observations stem from bulk heat transport. It is unlikely, as this would effectively increase N rather than diminish it [26].

In conclusion, we have observed the two opposite regimes of heat equilibration on the edge in the fractional QH regime, suggesting that exponential heat equilibration can occur at $\nu = 8/3$. Our result demonstrates the crucial importance of considering all downstream modes in the heat equilibration, particularly the integer ECs copropagating along the fractional edge modes. This is likely to impact experiments realizing new quantum circuits based on the nontrivial statistics of fractional QH states at $\nu > 1$.

We warmly thank C. Altimiras, A. Zhang, F. Pierre, A. Anthore, D. Kovrizhin, M. O. Goerbig, J. Splettstoesser and C. Spånslätt for enlightening discussions, as well as P. Jacques for precious technical assistance. This work was funded by the European Research Council (ERC-2018-STG *QUAHQ*), and by the "Investissements d'Avenir" LabEx PALM (ANR-10-LABX-0039-PALM). R. R.-P. and Y. H. acknowledge financial support form the European Research Council (ERC-2019-STG *TWISTRONICS*). P. R. acknowledges financial support form the European Research Council (ERC-2015-STG *COHEGRAPH*).

[1] C. W. J. Beenakker, Phys. Rev. Lett. **64**, 216 (1990).
[2] A. H. MacDonald, Phys. Rev. Lett. **64**, 220 (1990).
[3] C. L. Kane, M. P. A. Fisher, and J. Polchinski, Phys. Rev. Lett. **72**, 4129 (1994).
[4] C. L. Kane and M. P. A. Fisher, Phys. Rev. B **51**, 13449 (1995).
[5] C. L. Kane and M. P. A. Fisher, Phys. Rev. B **55**, 15832 (1997).
[6] A. Bid, N. Ofek, H. Inoue, M. Heiblum, C. L. Kane, V. Umansky, and D. Mahalu, Nature (London) **466**, 585 (2010).
[7] M. Dolev, Y. Gross, R. Sabo, I. Gurman, M. Heiblum, V. Umansky, and D. Mahalu, Phys. Rev. Lett. **107**, 036805 (2011).
[8] Y. Gross, M. Dolev, M. Heiblum, V. Umansky, and D. Mahalu, Phys. Rev. Lett. **108**, 226801 (2012).
[9] H. Inoue, A. Grivnin, Y. Ronen, M. Heiblum, V. Umansky, and D. Mahalu, Nat. Commun. **5**, 4067 (2014).
[10] V. Venkatachalam, S. Hart, L. Pfeiffer, K. West, and A. Yacoby, Nat. Phys. **8**, 676 (2012).
[11] M. Banerjee, M. Heiblum, A. Rosenblatt, Y. Oreg, D. E. Feldman, A. Stern, and V. Umansky, Nature (London) **545**, 75 (2017).
[12] M. Banerjee, M. Heiblum, V. Umansky, D. E. Feldman, Y. Oreg, and A. Stern, Nature (London) **559**, 205 (2018).
[13] S. K. Srivastav, R. Kumar, C. Spånslätt, K. Watanabe, T. Taniguchi, A. D. Mirlin, Y. Gefen, and A. Das, Phys. Rev. Lett. **126**, 216803 (2021).
[14] R. A. Melcer, B. Dutta, C. Spånslätt, J. Park, A. D. Mirlin, and V. Umansky, Nat. Commun. **13**, 376 (2022).
[15] I. Protopopov, Y. Gefen, and A. Mirlin, Ann. Phys. (Amsterdam) **385**, 287 (2017).
[16] C. Nosiglia, J. Park, B. Rosenow, and Y. Gefen, Phys. Rev. B **98**, 115408 (2018).
[17] K. K. W. Ma and D. E. Feldman, Phys. Rev. B **99**, 085309 (2019).
[18] C. Spånslätt, J. Park, Y. Gefen, and A. D. Mirlin, Phys. Rev. Lett. **123**, 137701 (2019).
[19] A. Aharon-Steinberg, Y. Oreg, and A. Stern, Phys. Rev. B **99**, 041302(R) (2019).
[20] K. K. W. Ma and D. E. Feldman, Phys. Rev. Lett. **125**, 016801 (2020).
[21] Y. Cohen, Y. Ronen, W. Yang, D. Banitt, J. Park, M. Heiblum, A. D. Mirlin, Y. Gefen, and V. Umansky, Nat. Commun. **10**, 1920 (2019).
[22] F. Lafont, A. Rosenblatt, M. Heiblum, and V. Umansky, Science **363**, 54 (2019).
[23] S. K. Srivastav, R. Kumar, C. Spånslätt, K. Watanabe, T. Taniguchi, A. D. Mirlin, Y. Gefen, and A. Das, arXiv:2202.00490.
[24] S. Jezouin, F. D. Parmentier, A. Anthore, U. Gennser, A. Cavanna, Y. Jin, and F. Pierre, Science **342**, 601 (2013).
[25] S. K. Srivastav, M. R. Sahu, K. Watanabe, T. Taniguchi, S. Banerjee, and A. Das, Sci. Adv. **5**, eaaw5798 (2019).
[26] See Supplemental Material at http://link.aps.org/supplemental/10.1103/PhysRevLett.129.116803 for detailed descriptions of the setup, calibration procedures, and measurements, as well as additional analysis and discussion, which includes Refs. [27–30].
[27] S. Kim, J. Nah, I. Jo, D. Shahrjerdi, L. Colombo, Z. Yao, E. Tutuc, and S. K. Banerjee, Appl. Phys. Lett. **94**, 062107 (2009).
[28] R. Ribeiro-Palau, S. Chen, Y. Zeng, K. Watanabe, T. Taniguchi, J. Hone, and C. R. Dean, Nano Lett. **19**, 2583 (2019).
[29] I. M. Flór, A. Lacerda-Santos, G. Fleury, P. Roulleau, and X. Waintal, Phys. Rev. B **105**, L241409 (2022).
[30] D. S. Wei, T. van der Sar, S. H. Lee, K. Watanabe, T. Taniguchi, B. I. Halperin, and A. Yacoby, Science **362**, 229 (2018).
[31] J. B. Pendry, J. Phys. A **16**, 2161 (1983).
[32] L. G. C. Rego and G. Kirczenow, Phys. Rev. B **59**, 13080 (1999).
[33] E. Sivre, H. Duprez, A. Anthore, A. Aassime, F. D. Parmentier, A. Cavanna, A. Ouerghi, U. Gennser, and F. Pierre, Nat. Commun. **10**, 5638 (2019).

[34] Z. Iftikhar, A. Anthore, S. Jezouin, F. Parmentier, Y. Jin, A. Cavanna, A. Ouerghi, U. Gennser, and F. Pierre, Nat. Commun. **7**, 12908 (2016).

[35] E. Sivre, A. Anthore, F. D. Parmentier, A. Cavanna, U. Gennser, A. Ouerghi, Y. Jin, and F. Pierre, Nat. Phys. **14**, 145 (2018).

[36] F. Amet, J. R. Williams, K. Watanabe, T. Taniguchi, and D. Goldhaber-Gordon, Phys. Rev. Lett. **112**, 196601 (2014).

[37] D. S. Wei, T. van der Sar, J. D. Sanchez-Yamagishi, K. Watanabe, T. Taniguchi, P. Jarillo-Herrero, B. I. Halperin, and A. Yacoby, Sci. Adv. **3**, e1700600 (2017).